J Mater Sci (2009) 44:5345–5353
DOI 10.1007/s10853-009-3442-7

FERROELECTRICS

On the triggering mechanism for the metal–insulator transition in thin film VO_2 devices: electric field versus thermal effects

Gokul Gopalakrishnan · Dmitry Ruzmetov · Shriram Ramanathan

Received: 19 February 2009 / Accepted: 25 March 2009 / Published online: 17 April 2009

Abstract Vanadium dioxide (VO_2) has been shown to undergo an abrupt electronic phase transition near 70 °C from a semiconductor to a metal, with an increase in dc conductivity of over three orders of magnitude, making it an interesting candidate for advanced electronics as well as fundamental research in understanding correlated electron systems. Recent experiments suggest that this transition can be manifested independent of a structural phase transition in the system, and that it can be triggered by the application of an electric field across the VO_2 thin film. Several experiments that have studied this behavior, however, also involve a heating of the VO_2 channel by leakage currents, raising doubts about the underlying mechanism behind the transition. To address the important question of thermal effects due to the applied field, we report the results of electro-thermal simulations on a number of experimentally realized device geometries, showing the extent of heating caused by the leakage current in the "off" state of the VO_2 device. The simulations suggest that in a majority of the cases considered, Joule heating is insufficient to trigger the transition by itself, resulting in a typical temperature rise of less than 10 K. However, the heating following a field-induced transition often also induces the structural transition. Nevertheless, for certain devices, we identify the possibility of maintaining the field-induced high conductivity phase without causing the structural phase transition: an important requirement for the prospect of making high-speed switching devices based on VO_2 thin film structures. Such electronically driven transitions may also lead to novel device functionalities including ultra-fast sensors or gated switches incorporating ferroelectrics.

G. Gopalakrishnan (✉) · D. Ruzmetov · S. Ramanathan
School of Engineering and Applied Sciences,
Harvard University, Cambridge, MA 02138, USA
e-mail: gokul@seas.harvard.edu

Introduction

Vanadium dioxide (VO_2) is known to undergo a structural phase transition (SPT) [1] at about 70 °C, that is closely accompanied by an abrupt change in resistivity and optical transmittance due to a metal-insulator transition (MIT) [2–8]. This transition temperature can be changed by tens of degrees by doping [9], making devices that can switch resistance very close to room temperature. Additionally, VO_2 thin films have been observed to exhibit a similar transition when an electric field on the order of 10^6 V/m is induced in it [10–12]. The mechanism of this field-induced transition, however, is under debate, and of particular significance is the question of whether or not the transition is triggered by Joule heating, and is thus induced via the SPT. Answering this question would facilitate a deeper understanding of the physics behind the electrically induced Mott transition in VO_2 as well as provide a better determination of the scope for utilizing VO_2 in high-speed electronic devices. A number of groups have explored the possibility of implementing ferroelectric field effect transistors (FFETs) [13, 14] where the channel semiconductor is a perovskite exhibiting a field effect, whose conductivity is tuned by a ferroelectric gate oxide. Similar applications for ferroelectrically tuned devices incorporating VO_2–based channels can be envisioned that make use of the large change in conductivity of a VO_2 thin film observed across its field-induced transition.

Experimental investigations addressing the role of Joule heating have been few. Kim et al. [15, 12] report Raman

measurements, in which the MIT is observed at a temperature that is lower than that for which the SPT is observed. This separation between the MIT and the SPT is also confirmed by microscopic X-ray diffraction measurements [16]. Sakai and Kurisu [17] report pressure dependence studies which indicate that the MIT is triggered independent of Joule heating. Lee et al. [18, 19] have measured the surface temperatures (in the range of 50–80 °C) by high resolution IR reflectance measurements, when large currents are driven through the film in the conducting state. While these measurements are valuable to the understanding of the mechanism involved in the MIT, a comprehensive investigation of the extent of Joule heating in a typical *I–V* measurement remains to be performed.

It is thus valuable to quantitatively explore the extent of heat generation and dissipation in the VO_2 thin film devices over the course of a transport measurement, to investigate whether Joule heating thermally induces a phase transition independent of or in addition to any field-induced effect. Stefanovich et al. [10], calculated a lower bound on the time required to raise the temperature of the VO_2 channel involved in current flow from the ambient, T_0 to the transition temperature, T_c, by ignoring any dissipation in the sample. This minimum rise time, t_{tr} is given by a simple heat balance expression, treating the VO_2 channel as an isolated system:

$$t_{tr} = \frac{C\rho_m\Omega_{ch}(T_c - T_0)}{VI}, \quad (1)$$

where $C = 690$ J/Kkg and $\rho_m = 4340\text{kg/m}^3$ are, respectively, the specific heat capacity and mass density [20] of VO_2, Ω_{ch} is the channel volume, V is the voltage applied across the channel, and I is the steady state current flowing through it. For a rectangular channel, as is typically the case in measurements of this kind, and a temperature difference $T_c - T_0 \approx 45$ K, this expression can be rewritten independent of the channel geometry, as $t_{tr} \approx 1.4 \times 10^8/(JE)$ (in SI units), where J and E are, respectively, the average values of the current density and electric field in the channel.

For the measurements of Stefanovich et al. [10], as well as several subsequent others [12, 17, 21, 22], this minimum rise time is on the order of 1 μs. While this number is not, by itself, a good approximation to the real rise time, it sets a useful lower bound on the time required to thermally induce a transition via an electric field. Consequently, observations of response to voltage switching at times on the order of nanoseconds or smaller [10, 22] strongly suggest that the transition is not triggered by Joule heating from leakage currents in the non-metallic state, particularly in those geometries where such rapid switching has been observed. However, in other measurements [12] where a significantly longer pulse width (or a continuous voltage) is employed during the measurement of $I-V$ characteristics, the role of Joule heating is undetermined. Moreover, for typical samples with heat capacity, $\mathcal{C}$, and thermal conductance $\mathcal{K}$, estimates of the thermal time constant, $\tau = \mathcal{C}/\mathcal{K}$ yield timescales on the order of nanoseconds. This suggests a strong role for dissipation, which would significantly constrain the temperature rise in the VO_2 channel, from that calculated in the above adiabatic limit.

In addition to the question of inducing a transition from the non-metal state, by Joule heating, is that of the temperature rise in the metallic state, and its influence on the measured *I–V* characteristics of these devices. Recent IR reflectance measurements by Lee et al. [18, 19] provide valuable information about local temperature rises in the range of 55–80 °C. Furthermore, despite the small length scales involved in these devices, elementary calculations of Joule heating using the Fourier heat transfer equation [18, 23, 24] have shown good agreement with measured data, and thus make the case for a more detailed evaluation.

In this paper we report detailed simulations of thermal effects in several experimentally studied VO_2 devices. These simulations draw upon the approach of Lee et al. [18] described above but involve a fuller consideration of both the electrical and thermal aspects of a number of measurements, as well as a complete incorporation of the device geometry. We thus compute the expected temperature rise in a number of experimentally realized devices under published measurement conditions, and directly address the question of whether or not the transition observed in these measurements is triggered by Joule heating.

Computation

We model the thermal phenomena in a number of VO_2–based devices using COMSOL Multiphysics® a finite element simulation environment. Materials specifications and experimental conditions have been replicated from literature, where available, or using reasonable extrapolations therefrom. Table 1 provides a list of some of the key device characteristics used for these simulations, as well as the maximum temperature rise in the non-metallic state determined for each device, under the experimental conditions reported (assuming the sample bottom surface is thermally anchored to the ambient).

The program numerically extracts solutions to the Fourier heat equation within each domain of the design structure. For an element of the system with thermal conductivity κ, specific heat C, and mass density ρ, the temperature T, is a solution to

Table 1 Simulated temperature rise (ΔT_{sim}) in the non-metallic state, in a number of experimentally realized devices, for the case where the bottom surface of the sample is thermally anchored to the ambient temperature

Device	Substrate	Channel (μm)	$V_c(V)$	I_A (mA)	ΔT_{sim} (K)
1 [12]	Si/SiO_2	0.09 × 25 × 5	16	0.2	6.5
2 [12]	Al_2O_3	0.09 × 50 × 3	20	0.5	7.5
3 [27]	Al_2O_3	0.10 × 50 × 20	21	0.4	3.5
4 [17]	Al_2O_3	0.22 × 1500 × 10	2.7	6	24
5 [21]	Al_2O_3	0.09 × 50 × 5	22	4.5	>40
6 [19]	Al_2O_3	0.06 × 50 × 15	2.5	1.0	0.1
7 [19]	Al_2O_3	0.06 × 50 × 15	13.5	1.5	1.0

Also included are some of the important simulation parameters taken from literature, namely the substrate material, VO_2 channel dimensions (thickness × width × length), voltage at the onset of the MIT (V_c), and the current in the non-metallic state, at this voltage

$$\rho C(\partial_t T) - \nabla \cdot (\kappa \nabla T) = \mathbf{J} \cdot \mathbf{E}, \quad (2)$$

where **J** and **E** are, respectively, the computed current density and electric field in the element and the entire system is subject to the appropriate initial and boundary conditions. For all surfaces exposed to atmosphere, the boundary condition for heat transfer is

$$\mathbf{n} \cdot (\kappa \nabla T) = h(T - T_0), \quad (3)$$

where **n** is the outward directed unit normal to the surface of interest, h is the heat transfer coefficient, and T_0 is the external temperature (set at 300 K for all the simulations reported here).

The current density and electric field are themselves numerically extracted from the voltage V, defined on the electrode surfaces, and the dc electrical conductivity σ, of each material in the device. The input parameters thus include the device geometry (dimensions of substrate, film, and electrodes), material properties (κ, ρ, C, σ) for VO_2, as well as the electrode and substrate materials and experimental conditions such as the applied voltage and thermal environment.

For $T-T_0 < 100$ K convective heat transfer to the surroundings exceeds any radiative heat loss, which scales like $(T-T_0)^4$ and diminishes rapidly for smaller temperature rises. We thus neglect radiative heat loss for all cases where $T-T_0$ is computed to be smaller than 50 K. This modeling further assumes that all surfaces and interfaces are perfectly flat and that the materials are both microscopically homogeneous as well as isotropic. As a result, our modeling does not account for non-uniformities in current flow, which are known to be prevalent in the high conductivity state of the VO_2 film [17]. We also assume that electrons in the channel are in thermal equilibrium with the lattice.

We explore a range of systems in these simulations, from those listed in Table 1 (devices described in the literature of field effect measurements in VO_2) to several others with varying properties. The geometry involved in all these simulations describes an in-plane device, with current flow along the plane of the VO_2 film. The vast majority of measurements investigating an electric field-induced transition have been performed in this device geometry [12, 17, 21, 22, 25–27], with similar film thicknesses ($H \approx 100$nm) but different channel lengths, L, and widths, W. In addition to simulations of the above samples we also explore the effect on heating of systematically varying the channel dimensions, thermal environment, substrate type, and voltage pulse widths.

Results and discussion

Experimental verification

In the low-temperature state ($T < T_c$), VO_2 is a conventional ohmic semiconductor for applied electric fields sufficiently smaller than the critical field. In this state, the resistance R, scales with the temperature of the film as $R \propto e^{\Delta E/k_B T}$, where ΔE is an activation energy and k_B is the Boltzmann constant. At room temperature, this typically gives rise to a halving of the film resistance from a temperature change as small as 20 K. For a VO_2 device with a large channel resistance, this resistance is hence very sensitive to the temperature of the film, with changes smaller than 0.1 K corresponding to measurable changes in resistance. A temperature rise induced by Joule heating would thus produce a resistance change in the film that could potentially be measured by a dc transport measurement. Specifically, one would expect an upward deviation from a linear I–V plot, corresponding to the heating-induced drop in resistance. Moreover, if this change in resistance, ΔR, is induced purely by heating, then ΔR for a given device should depend only on the applied voltage and be essentially independent of the device temperature.

We have observed such deviations from linearity in two-probe I–V measurements of high resistance devices grown by reactive sputtering (Ar + 8%O_2) of VO_2 on c-plane Al_2O_3 substrates, at substrate temperatures of about 550 °C [28]. Our channel geometries are significantly different from typical VO_2 devices, such as those listed in Table 1. In these devices, the channel length is greater than the channel width, in order to maximize the channel resistance and hence the sensitivity to temperature (typical channel dimensions are: length = 300 μm, width = 100 μm, and thickness = 100 nm). Such a geometry also ensures that for a given voltage applied between the terminals, the electric field is much smaller than in most other devices.

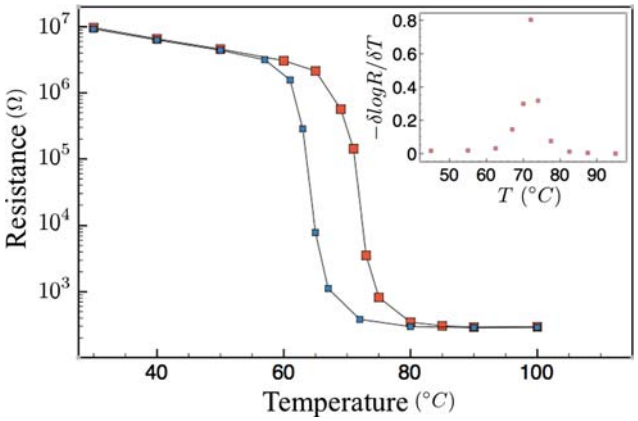

Fig. 1 Temperature dependence of resistance for a VO_2 device grown on c-plane Al_2O_3 substrate by reactive sputtering in an Ar/O_2 atmosphere at 550 °C. Resistances are measured for channel voltage, $V < 0.02$ V, to minimize Joule heat-induced temperature changes. The right and left traces (red and blue) are, respectively, the heating and cooling curves for the device. The inset shows a plot of $-\delta \log R/\delta T$ from the heating trace, indicating a transition at about 72° C. (Color figure online)

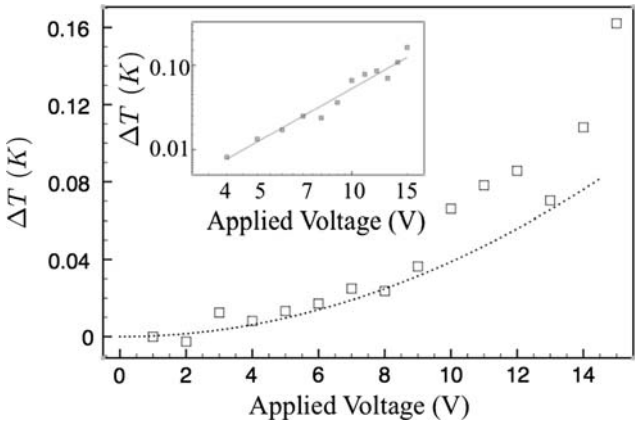

Fig. 2 Changes in film temperature extracted from measured changes in resistance (*open squares*) are plotted against the applied voltage. Simulated temperature rise for the same device is displayed as the dotted line. Inset: When plotted on a log-log scale, the temperature rise is best fit by the solid line representing $\Delta T \propto V^{2.1}$

Large contacts minimize the heat generated by the contact resistance, separately determined by four-probe measurements on Hall bar samples of similar dimensions. Figure 1 describes the temperature dependence of the low-current resistance (with $V < 0.1V$) of one such device during heating (red) and cooling (blue) sweeps, showing a change of over three orders of magnitude across the phase transition. The inset shows a sharp peak in $-\delta \log R/\delta T$ close to 72 °C for the heating trace, indicating the position of the transition temperature, T_c.

We measure voltage dependent resistance changes in this device, over a range of temperatures below T_c. Using the temperature dependence of resistance (at small currents; see Fig. 1) as a calibration curve, the change in resistance caused by Joule heating from larger currents can be used to estimate the temperature rise in the film as a function of applied voltage. Figure 2 shows a good agreement between this estimated temperature rise (open squares) for $V < 15$ V and the simulated temperature rise for this device in the steady state (dotted line). Furthermore, a log-log plot of the temperature rise against the voltage is well fit by a power law dependence given by $\Delta T \propto V^{2.1}$, which is in good agreement with the simulated dependence of $\Delta T \propto V^2$.

These temperature changes, in agreement with simulations, are measured to be essentially independent (with a variation of ±10%) of the device temperature through the range from 25 °C to 55 °C, over which the channel resistance itself changes by more than a factor of three. In these measurements, the voltage range was restricted to ensure that heating was the dominant source of deviation from linearity. At higher voltages, as the electric field approaches the critical field E_c, non-linearity due to the Poole-Frenkel effect becomes significant [11, 29]. For our range of voltages, the electric field in the channel is below 50 kV/m, which is significantly lower than E_c measured in these samples ($\sim 10^6$ V/m).

In addition to the above verification of our simulations of weak heating, we have also simulated the strong heating effects in the devices of Lee et al. [18, 19], and the results compare well with the surface temperatures directly measured by infrared reflectance in that study. We thus believe that our simulations are reasonably capable of reproducing the temperatures attained in other similar devices, during the course of *I–V* measurements.

Steady-state temperatures

Figure 3 is a schematic representation of the *I–V* characteristics extracted from a typical in-plane measurement using a voltage source and measuring the current produced in the device, with the sample and measurement geometry depicted in the inset. We simulate the results of heating, primarily for the conditions described by point A, where the VO_2 is still in the non-metallic state and the current through the channel is small, but also briefly examine heating at point B, where there is a large increase in conductivity from the transition, and the current in the film is thus significantly larger. Steady state temperatures are computed by setting $\partial_t T = 0$ in Eq. 2. As seen in Table 1, most measurements result in a steady state temperature that is below the transition temperature, thus confirming that a field assisted transition can be triggered independent of Joule heating. Only in the case of device 5 do we expect a temperature rise that would be large enough to induce the SPT.

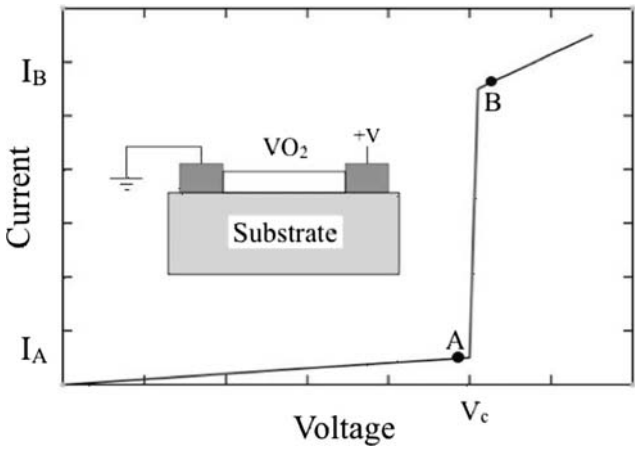

Fig. 3 Typical current–voltage characteristics of a two-terminal in-plane device, showing the applied voltage (V_c) at the onset of the transition, and the measured current in the non-metallic (I_A) and metallic (I_B) states, in the vicinity of the transition. The inset is a schematic representation of the device and measurement geometry: a voltage V is applied between two metallic electrodes straddling the VO_2 film and the resulting current is measured

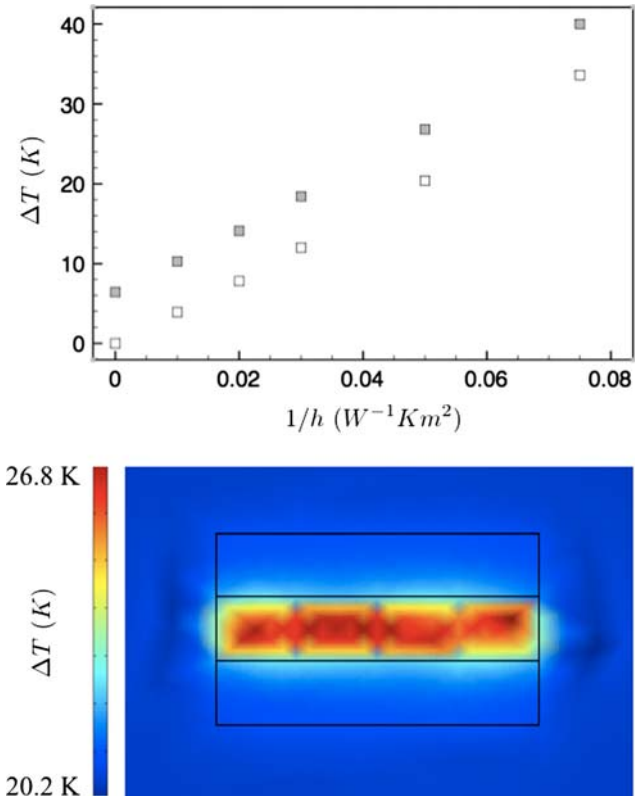

Fig. 4 *Top*: dependence of maximum (*filled squares*) and minimum (*open squares*) sample temperatures on the heat transfer coefficient, h (W/Km). The temperature rises are plotted against $1/h$ showing a linear dependence and a constant temperature gradient within the sample that is independent of h. *Bottom*: temperatures at the top surface of the substrate for device 2 (Table 1), showing the VO_2 channel in between the two metallic terminals

The commonly used substrates for measurement in this geometry are Si/SiO_2 [12, 25] and Al_2O_3 (c-plane) [12, 17–19, 21, 22, 25–27]. For the devices and measurements considered, the results of the numerical simulation of Joule heating show rather small steady-state temperature rises in the VO_2 channel, typically less than 10 K. Specifically, in the case where the device is assumed to be thermally shorted to a sample holder or the surface of a probe-station, so that one of its external surfaces is anchored to the ambient temperature ($T = 300$ K) while the remaining surfaces exchange heat to air via convection (with $h = 20$ W/Km^2), we find that the maximum temperature rise in the film corresponding to point A (in Fig. 3) is approximately 6.4 K for the Si/SiO_2 devices and 7.5 K for the Al_2O_3 devices in Ref. [12]. Even in the opposite extreme, where no part of the sample surface is in contact with a thermal sink (i.e., the entire sample is suspended in air) we find, for instance, that the film heats up by 27 K and 15 K for $h = 20$ W/Km^2 and $h = 50$ W/Km^2, respectively, in the Si/SiO_2 device.

The dependence of the temperature rise in the sample as a function of varying thermal environments is summarized in Fig. 4. This figure describes the steady state temperature rise at the hottest and coolest points on the sample, ΔT_{max} and ΔT_{min}, respectively, for different values of heat transfer to the surroundings ($h > 10$ W/Km^2). Not surprisingly, the temperature rises are linear in $1/h$ for small values of ΔT (since the steady state power loss, $h\Delta T$ is simply the power generated by the current), and show upward deviations from linearity for larger ΔT which arise from the temperature dependence of the channel resistivity. The temperature gradient within the sample is itself independent of the boundary conditions and depends on the applied voltage and the material properties. The lower part of this figure shows the simulated temperature distribution in device 1 along a horizontal plane lying just below the VO_2 film, for the case where $h = 20$ W/Km^2 for all surfaces (simulating a worst case situation where the sample is essentially suspended in air with no thermal shorts to a heat sink); the three rectangular features visible are the VO_2 channel, and the two metallic terminals (of dimensions 25μm × 5 μm, as described in Table 1).

On the other hand, as long as some part of the outer surface is set at the ambient temperature, the simulated temperature rise is essentially independent of the choice of h, for values in the range of $h = 10-100$ W/Km^2, which are typical for convective heat transfer to air [30]. It is also only weakly dependent on the size of the substrate chip, which we have chosen as a 2 mm × 2 mm square with 500 μm thickness.

To study the role of the channel size, we simulate the heating effects for channel dimensions ranging from 100 nm to 100 μm, when the device is in the non-metallic

state (at point A, in Fig. 3). Over this range of dimensions, we assume that the current density and electric field at the onset of the transition remain constant. From the range of experiments involved, we note, however, that these values typically vary by about an order of magnitude. For this series of simulations, we use the values measured by Kim et al. [12], for measurements on the Si/SiO_2 device, namely: $E_c = V_c/L \approx 3 \times 10^6$ V/m and $J_A \approx 10^4$ A/cm^2.

Figure 5 shows the maximum steady state temperature rise in the film (under conditions corresponding to point A) as a function of the channel width W (solid line), and the channel length, L (squares). We find a weak reduction in the temperature rise for narrower channels, resulting from a decrease in the channel current, which is proportional to the channel width. The weakness of the decrease arises from the decreasing mass of the VO_2 film, which partially offsets the effect of the reduced current. A similar decrease is observed for channels with smaller lengths, arising from the reduction in applied voltage required to achieve a given critical field. Despite the weakness of dependence on the channel dimensions, it is noteworthy that the temperature rise from Joule heating may be suppressed by nearly an order of magnitude by shrinking the channels from about 20 μm in size to the vicinity of 200 nm. It should hence be possible to make devices with small temperature rises, even if the critical field for the film is large, simply by an appropriate choice of the channel dimensions and moderate heat sinking.

We also note, in these simulations, the effect of the substrate material. Between the choices of an Si/SiO_2 substrate and an Al_2O_3 substrate, we find little difference in the resulting temperature rise given similar properties of the VO_2 film and similar channel dimensions. While the first choice of substrate carries the advantage of a large thermal conductivity from Si ($\approx$160 W/Km), this benefit is completely offset by the SiO_2 film, which has a very poor thermal conductivity (approximately 1 W/Km). The Al_2O_3 substrate, on the other hand, has a good, but intermediate value of thermal conductivity (typically about 45 W/Km), which makes it a better choice if the thickness of the SiO_2 is in excess of 200 nm but a poorer choice for oxide films thinner than 50 nm. For oxide layers of thickness between these values, the two substrates give rise to comparable temperature rises for comparable device properties. The images in Fig. 6 show the steady-state temperature distribution in the two types of devices measured by Kim et al. [12] (conditions described in Table 1). The first is for the Si/SiO_2 (200 nm) substrate, showing a confinement of the high temperatures in the vicinity of the channel by the poorly conducting oxide. The second is for the device with an Al_2O_3 substrate where the temperature gradient is significantly more homogeneous and isotropic. Nevertheless, the steady-state film temperatures computed for these two devices are similar. This series of simulations also reveals the effect of a poor thermal contact between the film and the substrate. Specifically, introducing an interface with

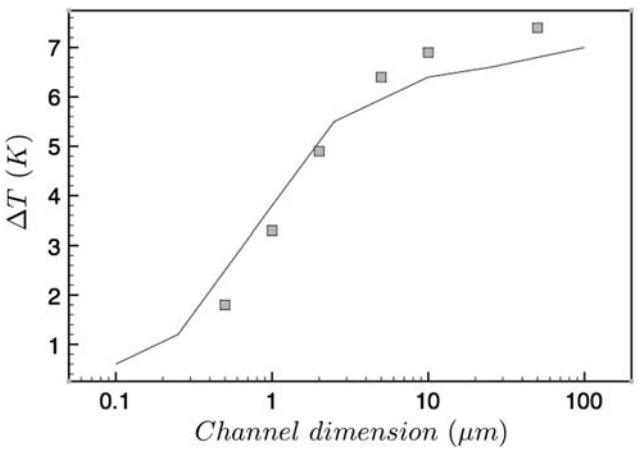

Fig. 5 Maximum temperature rise in the film, for conditions corresponding to point A of Fig. 3, as a function of the channel width (*solid line*), W, for a fixed channel length, and the channel length (*squares*), L, for a fixed width

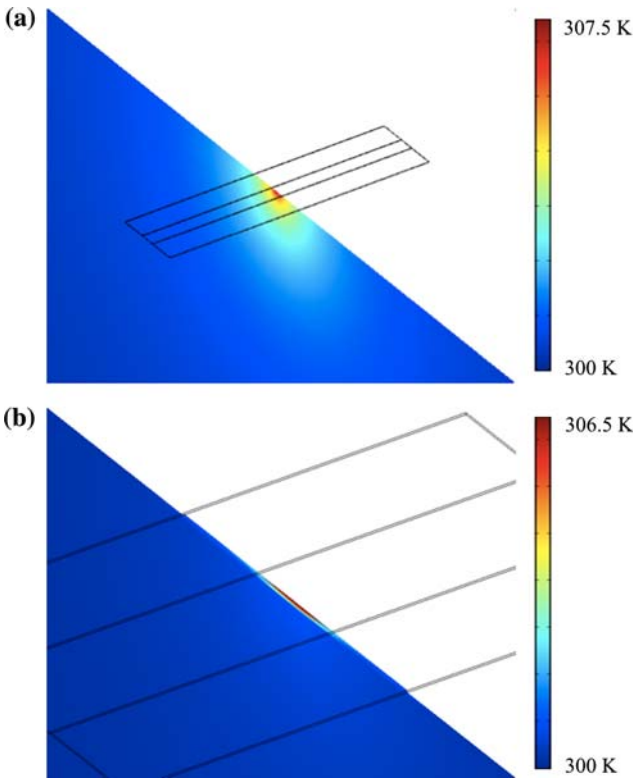

Fig. 6 Simulated temperature distributions along a vertical slice through the sample (only region near the channel is depicted) in devices 1 and 2 [12] of Table 1. **a** The substrate is c-plane Al_2O_3 (device 2), and the temperature distribution is seen to be highly isotropic through the substrate. **b** When the substrate is Si/SiO_2 (200 nm) (device 3), the poorly conducting SiO_2 layer maintains a large thermal gradient (in the vertical direction) across its thickness

thermal conductivity over an order of magnitude lower than that of the VO_2 gives rise to a significant increase in the film temperatures only if this interface is several tens on nm thick.

Another important point here is that the temperature rise is strongly dependent on the conductivity of the film, which in turn, is very sensitive to the growth conditions [31]. The variability in film conductivity, therefore, can result in temperature rises that are a few times bigger or smaller than those simulated. More importantly, for a measurement using a voltage source, the temperature rise in the film just beyond the transition (point B of Fig. 3) is significantly greater, due to the large increase in conductivity, than when the film is still in the non-metallic state (point A). Thus, for instance, in the measurement of Kim et al. [12] on the Si/SiO_2 device, the order of magnitude increase in conductivity from the transition produces a temperature rise of over 60 K when the film is conducting (point B) compared to a rise of only about 6.5 K at point A. It is therefore likely that a field-induced transition is rapidly followed by a thermal phase transition, which is in agreement with micro-Raman spectroscopy studies [21] showing that the electronic phase transition precedes the structural phase transition. This point may also have a direct significance for the large hysteresis observed by Kim et al. [12], in *I–V* measurements. While in most of the device simulations, the heating in the non-metallic state appears insufficient to itself trigger a thermally induced transition, the heating in the metallic state is sufficient to keep the system in this state even if the drive voltage is reduced considerably. This may explain such a large hysteresis, where the VO_2 remains metallic even as the field is decreased to values as small as roughly half the critical field.

Finally, we consider the role of the ambient temperature, specifically on the prospect of developing devices in which the Joule heating, even in the conducting state induced by an applied voltage, is small enough that it is insufficient to trigger the temperature-induced SPT. We consider the example of device 3 of Kim et al. [27], where the simulated temperature rise at point A is 3.5 K, with the ambient temperature $T_0 = 300$ K and the critical voltage at this temperature is roughly 21 V. At point B, just beyond the field-induced transition, we find that the increase in the film conductivity results in a much larger temperature rise of approximately 70 K. Thus, according to this simulation, the field-induced transition at $T_0 = 300$ K should be closely accompanied by a thermally induced transition, since the transition temperature for this device was measured to be $T_c \approx 340$ K. However, Kim et al. observed a stable intermediate phase at $T_0 = 300$ K over a narrow range of voltages. Our simulation of this device thus overestimates the temperature rise in the film (by approximately a factor of two), which is not unexpected, given the uncertainties in the device properties (especially the nature of the contact resistance, which is poorly characterized in this regime) and the thermal environment.

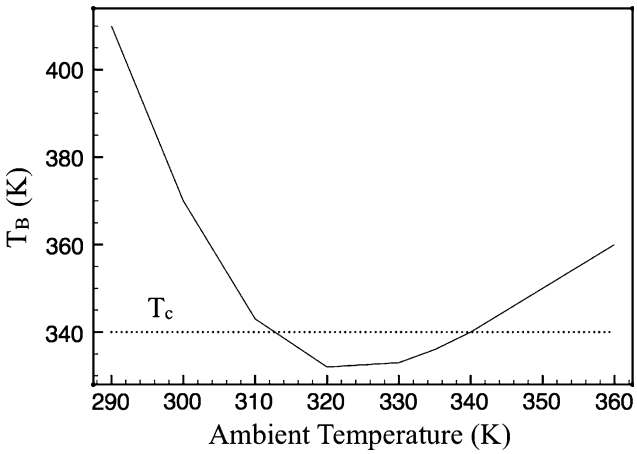

Fig. 7 Maximum temperature induced within device 3 in the conducting state (point B of Fig. 3) as a function of the ambient temperature, when the applied voltage just exceeds the critical voltage. The horizontal dotted line represents the approximate transition temperature for this device, revealing the range of temperatures over which $T_B < T_c$

We follow this up by a broader exploration of the temperature of the film at point B, as a function of T_0, to determine the range of ambient temperatures for which $T_B < T_c$, so that the SPT is never triggered, even after the device switches to the high conductivity state. Figure 7 describes the results of these simulations on device 3, showing the Joule heat-induced steady-state temperature when the device is in the field-induced high conductivity state (point B). The non-monotonicity in T_B is a result of the competition between the increasing ambient temperature, T_0 and the decrease in the critical voltage V_c, as the ambient temperature approaches T_c. We find that a stable high conductivity state with monoclinic structure would exist over a narrow range of temperatures above 310 K, up to the transition temperature of 340 K. This result is in general agreement with the experiment, though the range of temperatures is somewhat smaller than the actual range observed by Kim et al. [27].

Transient behavior

Temporal evolution of the temperature changes in the VO_2 film is a valuable aspect of the Joule heating in these devices. Within the non-dissipative calculation used by Stefanovich [10] and others, the temperature rises linearly with time, from the instant the voltage is applied, resulting in a finite rise time for any given temperature change. As seen from the steady state analysis, however, the temperature in a dissipative system saturates at values which are

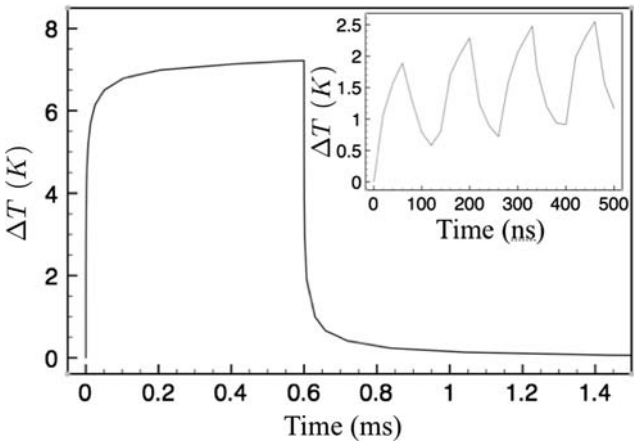

Fig. 8 Temperature rise in the VO_2 film for a pulsed voltage applied to device 2 (of Table 1). A voltage of 20 V is switched on at $t = 0$, and switched off at $t = 600$ μs. The inset shows the temperature rise as in the same device, over the first few cycles of a pulsed measurement, for a much shorter pulse of width = 64 ns at 50% duty cycle

often smaller than the transition temperature, far from the expectation that the transition temperature be reached within a μs of applying typical voltages. The time dependence in these systems is thus expected to differ significantly from that estimated within the non-dissipative approximation, motivating an examination of the transient behavior of temperatures following a switching (on or off) of the applied voltage.

Figure 8 depicts the temperature changes in device 2 (see Table 1) as a function of time, during a voltage pulse, with an "on" time of 600 μs. The time taken to cover 90% of the steady-state temperature rise (which is 7.5 K) is about 100 μs, which is nearly three orders larger than the estimate from the non-dissipative calculation. However, the time to achieve 30% of this steady-state rise is only about 100 ns, which is much closer to the non-dissipative estimate. The absence of a single, characteristic time constant for the system is due to the two primary heat transfer processes involved: dissipation of heat from the VO_2 film through the substrate and convective heat loss to the ambient, from the outer surfaces of the device. As we find from simulations where one or the other of these processes is suppressed, the thermal dissipation through the substrate dominates the temperature response over short time scales, while the heat transfer to surroundings is important only for the long time behavior.

From these transient simulations, we find that in order to significantly reduce the effect of Joule heating (in those cases where it is significant) by using a pulsed voltage, it is necessary to restrict the pulse width to values no greater than tens of ns. One such case is depicted in the inset of Fig. 8, which shows the temperature rise over the first few cycles of a 60 ns pulsed voltage (at 50% duty-cycle); the steady-state rise for this device is about 7.5 K. It is thus only possible to significantly affect the maximum temperature rise in the film by varying the on-time of a pulsed voltage within the regime of ns.

Furthermore, in many cases, where the electrically induced transition also leads to a thermal phase transition due to heating in the high conductivity state, we find that the film temperature drops back below the transition temperature over times as long as tens of μs following the switching off of the voltage pulse. It is thus valuable, for potential application in high-speed switching devices, to be able to induce the electronic phase transition without also effecting a structural phase transition.

Conclusions

In this paper, we report extensive numerical simulations of heat generation and dissipation in a number of experimentally studied VO_2 thin film devices. The device geometries, materials properties and experimental conditions are taken from papers describing observations of an electric field-induced transition in VO_2. We find that in most cases, the steady-state temperature reached by the VO_2 film from heating in the non-metallic state is below the transition temperature, thus supporting a mechanism where the electronic phase transition is induced by an applied electric field, rather than purely from Joule heating in the current channel. For a majority of the measurements that were simulated, this temperature rise at the observed onset of the field-induced transition is found to be below 10 K.

In most devices, however, when the current is driven by a voltage source, the increased Joule heating following this transition produces simulated film temperatures that are tens of degrees above T_c, pointing to an SPT that closely accompanies the field-induced transition. Nevertheless, we demonstrate and discuss the existence of device geometries, material parameters, and thermal conditions under which it could be possible to induce an electronic phase transition without also triggering the SPT thermally. These results are of importance to questions about the suitability of VO_2 for use in a new generation of high-speed electronic devices such as optical switches, FETs, and FFETs, in which a traditional semiconductor element is replaced by a correlated oxide material.

Acknowledgements This work was supported by AFRL-WPAFB and NSF-SIA Supplement to the Nanoscale Science and Engineering Initiative under NSF Award Number PHY-0601184. Device fabrication was performed, in part, at the Harvard University Center for Nanoscale Systems (CNS), a member of the National Nanotechnology Infrastructure Network (NNIN), which is supported by NSF Award No. ECS-0335765.

References

1. Morin FJ (1959) Phys Rev Lett 3:34
2. Zylbersztejn A, Mott NF (1975) Phys Rev 11:4383
3. Berglund CN, Guggenheim HJ (1969) Phys Rev 185:1022
4. Mott NF (1990) Metal-insulator transition. Taylor and Frances, London
5. Goodenough JB (1971) J Solid State Chem 3:490
6. Imada M et al (1998) Rev Mod Phys 70:1039
7. Cavalleri A et al (2001) Phys Rev Lett 87:237401
8. Cavalleri A et al (2004) Phys Rev B 70:161102
9. Xu S et al (2004) J Mater Sci 39:489. doi:10.1023/B:JMSC.0000011503.22893.f4
10. Stefanovich G et al (2000) J Phys Condens Matter 12:8837
11. Boriskov PP et al (2002) Tech Phys Lett 28:406
12. Kim HT et al (2004) New J Phys 6:52
13. Watanabe Y (1995) Appl Phys Lett 66:1770
14. Mathews S et al (1997) Science 276:238
15. Kim HT et al (2006) Phys Rev Lett 97:266401
16. Kim BJ et al (2008) Phys Rev B 77:235401
17. Sakai J, Kurisu M (2008) Phys Rev B 78:033106
18. Lee JS et al (2007) Appl Phys Lett 90:015907
19. Lee JS et al (2007) Appl Phys Lett 91:133509
20. Samsonov GV (1987) The oxide handbook. IFI/Plenum, New York
21. Kim HT et al (2005) Appl Phys Lett 86:242101
22. Okimura K, Sakai J (2007) Jpn J Appl Phys 46:813
23. Berglund CN (1969) IEEE Trans Electron Devices 16:432
24. Duchene J et al (1971) Appl Phys Lett 19:115
25. Chae BG et al (2004) J Korean Phys Soc 44:884
26. Youn DH et al (2004) J Appl Phys 95:1407
27. Kim BJ et al (2007) Appl Phys Lett 90:023515
28. Ruzmetov D et al (2008) Phys Rev B 77:195442
29. Ko C, Ramanathan S (2008) Appl Phys Lett 93:252101
30. Lasance C, Moffat C (2005) Elec Cool 11:4
31. Mlyuka NR, Kivaisi RT et al (2006) J Mater Sci 41:5619. doi:10.1007/s10853-006-0261-y